

## Thermal shock resistance and thermal expansion behavior of $\text{Al}_2\text{TiO}_5$ ceramics prepared from electrofused powders

Ik Jin Kim\*

Institute for Processing and Application of Inorganic Materials, PAIM, Dept. of Mat. Science and Engineering, Hanseo University, 360, Daegok-ri, Seosan, Chungnam 352-820, Korea

Aluminium titanate ( $\text{Al}_2\text{TiO}_5$ ) with an excellent thermal shock resistant and a low thermal expansion coefficient was obtained by solid solution with  $\text{MgO}$ ,  $\text{SiO}_2$ , and  $\text{ZrO}_2$  in the  $\text{Al}_2\text{TiO}_5$  lattice or in the grain boundary solution through electrofusion in an arc furnace. However, these materials have low mechanical strength due to the presence of microcracks developed by a large difference in thermal expansion coefficients along crystallographic axes. Pure  $\text{Al}_2\text{TiO}_5$  tends to decompose into  $\alpha\text{-Al}_2\text{O}_3$  and  $\text{TiO}_2$ -rutile in the temperature range of 750~1300°C that render it apparently useless for industrial applications. Several thermal shock tests were performed: Long term thermal annealing test at 1100°C for 100 hrs; Cyclic thermal shock in a two chamber furnace between 750 and 1400°C for 100h; and water quenching from 950°C to room temperature (RT). Cyclic thermal expansion coefficients up to 1500°C before and after decomposition tests was also measured using a dilatometer. Changes in the microstructure, thermal expansion coefficients, Young's modulus and strengths were determined. The role of microcracks in relation to thermal shock resistance and thermal expansion coefficient is discussed.

### Introduction

Aluminium titanate ( $\text{Al}_2\text{TiO}_5$ ) is well-known as an excellent thermal shock resistant material, because of its low thermal expansion, low thermal conductivity and low Young's modulus. These properties allow for its testing as an insulating material in engines, for portliners, piston bottoms, and turbochargers [1]. However,  $\text{Al}_2\text{TiO}_5$  materials have low mechanical strength because of microcracks induced by the high anisotropy of the thermal expansion coefficient along the crystallographic axes [2, 3]. Unstabilized  $\text{Al}_2\text{TiO}_5$  tends to decompose into  $\alpha\text{-Al}_2\text{O}_3$  and  $\text{TiO}_2$  in the temperature range of 800-1300°C [4, 5].

The decomposition occurs when adjacent aluminium and titanium octahedra collapse because the lattice site occupied by the aluminium is too large [6]. The available thermal energy permits the aluminium to migrate from its position, and results in a structural dissolution to rutile and corundum [7]. Following the decomposition, the material neither exhibits a low thermal expansion coefficient nor favorable thermal shock behavior, that render it apparently useless for industrial applications.

The thermal instability of  $\text{Al}_2\text{TiO}_5$  can be recovered from solid solution with  $\text{MgO}$ ,  $\text{Fe}_2\text{O}_3$ , or  $\text{Cr}_2\text{O}_3$  in the  $\text{Al}_2\text{TiO}_5$  lattice, which are isomorphous with the mineral Pseudobrookite, such as  $(\text{Fe}_2\text{TiO}_5)$ ,  $\text{MgTi}_2\text{O}_5$ , or

$(\text{Al,Cr})_2\text{TiO}_5$ .  $\text{Al}_2\text{TiO}_5$  can be also kinetic stabilized by limitation of grain growth. Another source of stabilization is the formation of microcracks by the addition of additives such as  $\text{SiO}_2$ ,  $\text{ZrO}_2$ ,  $\alpha\text{-Al}_2\text{O}_3$ , or mullite, most of which do not form solid solution with  $\text{Al}_2\text{TiO}_5$  but rather restrain the tendency of  $\text{Al}_2\text{TiO}_5$  towards decomposition [8].

Stabilized  $\text{Al}_2\text{TiO}_5$  components in engines normally are surrounded with liquid aluminium or cast iron, and the combination of ceramic and metal materials requires a very good constructive adaptation of the two elements. During solidification of the metal melt, very high stresses act on the ceramic, because of the significantly higher thermal expansion of the metals. Therefore, a certain elasticity is necessary in order to avoid damage to the ceramic parts when they are surrounded by metals. The anisotropy of the elasticity and the thermal expansion coefficient between the ceramic and the metal cause microcracks in  $\text{Al}_2\text{TiO}_5$  ceramics; in turn, the cracks act as a stress absorber, in which the open crack flanks are closed during solidification of the molten metal [9].

In the present study, the solid solution of  $\text{Al}_2\text{TiO}_5$  was synthesized by substitution  $\text{Al}^{3+}$  or  $\text{Ti}^{4+}$  ion by  $\text{Mg}^{2+}$ ,  $\text{Zr}^{4+}$  and  $\text{Si}^{4+}$  ions. The relation between microstructure, thermal expansion coefficient and thermal shock resistance after sintered various temperature was discussed.

### Experimental

The powders were prepared though electrofusion in an arc furnace. Table 1 lists the chemical composition

\*Corresponding author:  
Tel: +82 (041) 660-1441  
Fax: +82 (041) 688-7375  
E-mail: ijkim@hanseo.ac.kr



of powders. ATG1 and 2 were unstabilized  $\text{Al}_2\text{TiO}_5$  whereas ATG3 and ATG4 were stabilized during the fusion process though addition of  $\text{MgO}$ . The later two compositions both contain small amounts of  $\text{ZrO}_2$  but differ in their  $\text{SiO}_2$  content. All powders in the as received condition were milled and separated and below 4  $\mu\text{m}$  in grain size with an average particle size of 2.5  $\mu\text{m}$ . The specific surface area (BET) of all materials were 2.3  $\text{m}^2/\text{g}$ . Tests samples of various sizes were prepared by die pressing under following conditions: 3% Zusoplast 126/3 as plastifer, 5% optapix PAF 35 as binder, 5%  $\text{H}_2\text{O}$ , granulated by sieve granulation and cold pressed at 100  $\text{N}/\text{mm}^2$ . The firing was carried out following conditions;

- Room temperature  $\sim 500^\circ\text{C}$ : 100 $^\circ\text{C}/\text{h}$
- 500 $^\circ\text{C}$ : 2h, soaking time
- 500 $^\circ\text{C}$   $\sim$  to max. temp. (1500 $^\circ\text{C}/2\text{h}$ ): 30 $^\circ\text{C}/\text{h}$
- Sintering temperature  $\sim 600^\circ\text{C}$ : 600 $^\circ\text{C}/\text{h}$
- 600 $^\circ\text{C}$   $\sim$  room temperature

The thermal shock resistance of the subject materials was determined according to a water quenching process by way of analogy to a German industrial standard [10]. Three specimens per materials were heated to 950 $^\circ\text{C}$  for 15 mins in a muffle furnace and quenched with flowing water to 20 $^\circ\text{C}$  for 15 mins. After drying at 110 $^\circ\text{C}$  for 30 mins, all specimens that withstood the thermal shock without spontaneously developing major cracks were subjected to the following tests in the cold condition: The 3-point-bending of specimens (7  $\times$  7  $\times$  70 mm) at room temperature was measured by universal-type testing machine. The span length was 40 mm and the cross head speed was 0.2 mm/min. The high temperature bending strength measurements in air used a special sample holder giving slightly lower strength values due to frictional effects. The adiabatic young's modulus was measured by the resonance frequency method as a function of the number of quenching cycles, using bending specimens. The thermal expansion was determined on specimens (25  $\times$  5  $\times$  5 mm), heating and cooling rate 5 $^\circ\text{C}/\text{min}$  in air by dilatometer. In order to evaluate the thermal durability of the various composition, the following tests were carried out;

**Table 1.** Chemical Composition of ATG\* Composites (wt%)

Materials	ATG1	ATG2	ATG3	ATG4
$\text{Al}_2\text{O}_3$	55.50	70	80	00
$\text{TiO}_2$	43.90	43.90	32.75	40.00
$\text{ZrO}_2$	0.05	0.40	3.00	2.30
$\text{SiO}_2$	0.15	0.30	7.90	1.20
$\text{MgO}$	—	—	2.10	3.00
$\text{Fe}_2\text{O}_3$	0.20	0.50	0.20	0.25
$\text{Na}_2\text{O}$	0.20	0.20	0.20	0.20
$\text{CaO}$	0.01	0.01	< 0.05	< 0.05

\*ATG: Powder of dynamic nobel chemicals, D-5210 troisdorf.

1) Cyclic thermal shock in a two chamber furnace between 750-1400-750 $^\circ\text{C}$ . The total number of cycles was 23 with a cyclic interval of 100 hrs,

2) Long term thermal annealing test at 1100 $^\circ\text{C}$  for 100 hrs.

3) Cyclic thermal expansion coefficients up to 1500  $^\circ\text{C}$  before and after decomposition tests was also measured using a dilatometer.

The thermal shock resistance was theoretically calculated by the thermal stress parameters  $R_1$  and  $R_2$ .

$$R_1 = \frac{\sigma_{br}(1-\gamma)}{\alpha E} \quad (1)$$

$$R_2 = R_1 \times \lambda \quad (2)$$

Where  $R_1$  and  $R_2$  are a material constant that can be described as a material resistance factor for thermal stresses,  $\sigma_{br}$  is the flexural strength,  $E$  is Young's modulus,  $\alpha$  is the thermal expansion coefficient,  $\gamma$  is Poisson's ratio, and  $\lambda$  is the thermal conductivity, which is assumed to be constant ( $\gamma = 0.24$ ,  $\lambda = 1.5 \text{ W/mk}$ ) in this study [10].

## Results and Discussion

The physical properties of the sintered specimens at 1500 $^\circ\text{C}$  for 2 hrs are given in Table 2. The physical properties can be adjusted over in a wide range: apparent density 3.61~3.68  $\text{g}/\text{cm}^3$ , thermal expansion coefficient (TEC, RT-1000 $^\circ\text{C}$ ) 1.3~3.0  $\times 10^{-6} \text{ K}^{-1}$  and bending strength 25~49 MPa. The relative density of pure  $\text{Al}_2\text{TiO}_5$  (ATG1) was only 92.1% of theoretical. Because the densities of the starting oxides  $\alpha\text{-Al}_2\text{O}_3$  and  $\text{TiO}_2$  (rutile) are 3.99 and 4.25  $\text{g}/\text{cm}^3$ , respectively. Therefore, the formation of pseudobrookite type  $\beta\text{-Al}_2\text{TiO}_5$  with a theoretical density of 3.70  $\text{g}/\text{cm}^3$  is accompanied by an about 11% molar volume increase. Relatively high temperature strength of 98.0 MPa at 1100 $^\circ\text{C}$  was found in ATG3 having 7.90 wt% of  $\text{SiO}_2$ .

**Table 2.** Physical Data of the Sintered Specimens

Physical Data	ATG1	ATG2	ATG3	ATG4
Green density ( $\text{g}/\text{cm}^3$ )	2.10	2.16	2.11	2.15
Raw density ( $\text{g}/\text{cm}^3$ )	3.39	3.43	3.44	3.49
True density ( $\text{g}/\text{cm}^3$ )	3.68	3.68	3.61	3.67
Relative density (%)	92.1	93.2	95.3	95.1
Apparent density (%)	—	3.98	3.7	4.7
Total density (%)	7.9	6.8	4.7	4.9
Firing shrinkage (%)	15.5	15.4	15.0	15.1
Coefficient of thermal expansion (1/K $\times 10^{-6}$ , RT-1273K)	—	3.0	2.3	1.3
Thermal expansion, RT-1273K (%)	—	0.35	0.28	0.22
Bending strength (MPa)	—	25.0	50.0	29.0
Hot MOR (MPa)				
800 $^\circ\text{C}$	—	28.0	60.0	58.0
1100 $^\circ\text{C}$	—	43.0	98.0	90.0
1300 $^\circ\text{C}$	—	38.0	50.0	48.0



This result can be attributed to the formation of grain boundary liquid phase and progressive fine grain microcrack-healing of all materials with increasing temperature has also its good effect on bending strength.

Pure  $\text{Al}_2\text{TiO}_5$ , i.e. ATG1 and ATG2 exhibits an inhomogeneous broad grain size of  $\beta\text{-Al}_2\text{TiO}_5$  between about 5–10  $\mu\text{m}$  and 5–20  $\mu\text{m}$  with a small amount of dispersed corundum phase, respectively, in Fig. 1. Intergranular cracks were noticed, preferentially between larger grain, as a consequence of the known anisotropy of  $\beta\text{-Al}_2\text{TiO}_5$ .<sup>11</sup> The interparticle bonding of ATG1 and ATG2 is apparently loose due to the presence of microcracks created in the cooling step and poor sinterability of pure  $\text{Al}_2\text{TiO}_5$ . In all cases, the tialite grains sizes are surrounded by grain boundary microcracks. According to the dilatometric measurements up to 1000°C the total linear expansion of ATG materials did not exceed the value of 0.35%. This is in good agreement with the data obtained in the investigation of expansion. These low expansion values during heating could be ascribed to the process of recombination of grain boundaries, i.e. microcracks, created during previous cooling phases of sintering, closing. When compared with microstructure of ATG1 and ATG2, the stabilized specimens ATG3 and ATG4 appear to have a smaller mean grain size  $\beta\text{-Al}_2\text{TiO}_5$  having grain spheroidization and neck formation between particles of  $\beta\text{-Al}_2\text{TiO}_5$ . It was more pronounced in samples (ATG3) with a higher  $\text{SiO}_2$  content in Fig. 1.

The thermal shock behavior under cyclic conditions

between 750–1400°C shows no change in microstructure and phase assemblage for all three specimens in Fig. 3. After the thermal durability test at 1100°C for 100 hrs, ATG2 materials decompose completely to its components corundum and rutile. However, approximately 20% of the aluminium titanate in ATG3 and ATG4 is still retained in the undercomposed state. Thus in order to prevent decomposition of the stabilized material the critical temperature range between about 800–1300°C must be traversed within a short period of time. The change in the phase compositions due to cyclic thermal shock and thermal loading tests are given in Table 3.

The maximum thermal expansion of the materials studied occurs between 1100 and 1300°C. The thermal expansion coefficient of ATG2, ATG3 and ATG4 lies between 0.35 and  $3.0 \times 10^{-6} \text{ K}^{-1}$  in the temperature range 100–1000°C. This can be compared with a theoretical expansion coefficient for single phase  $\beta\text{-Al}_2\text{TiO}_5$  of  $9.7 \times 10^{-6} \text{ K}^{-1}$ . It is the pronounced thermal expansion anisotropy of the individual  $\text{Al}_2\text{TiO}_5$  grains that gives rise to internal stresses on a microscopic scale during cooling from the firing temperature. These localized internal stresses are the driving force for microcrack formation. During reheating run, the individual crystallites expand at the lower temperatures, thus the solid volume of sample expands to the smaller sized microcracks, while the macroscopic dimensions remain almost constant. As a result, the material expands very little. The higher the temperature, the more

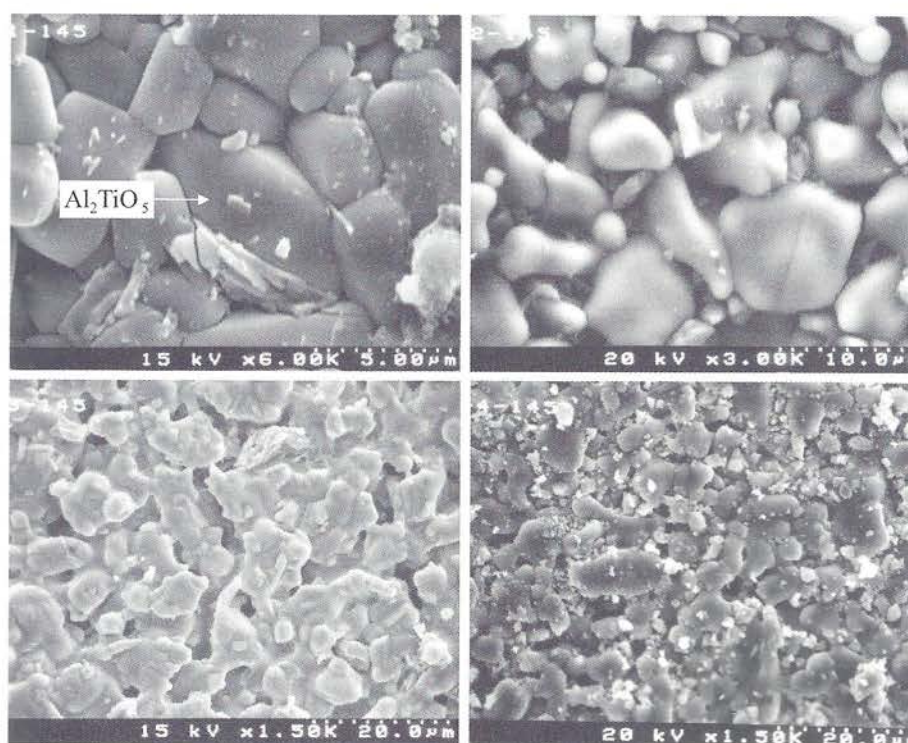


Fig. 1. Microstructure of sintered ATG1, 2, 3 and 4 at 1450°C for 2hrs.



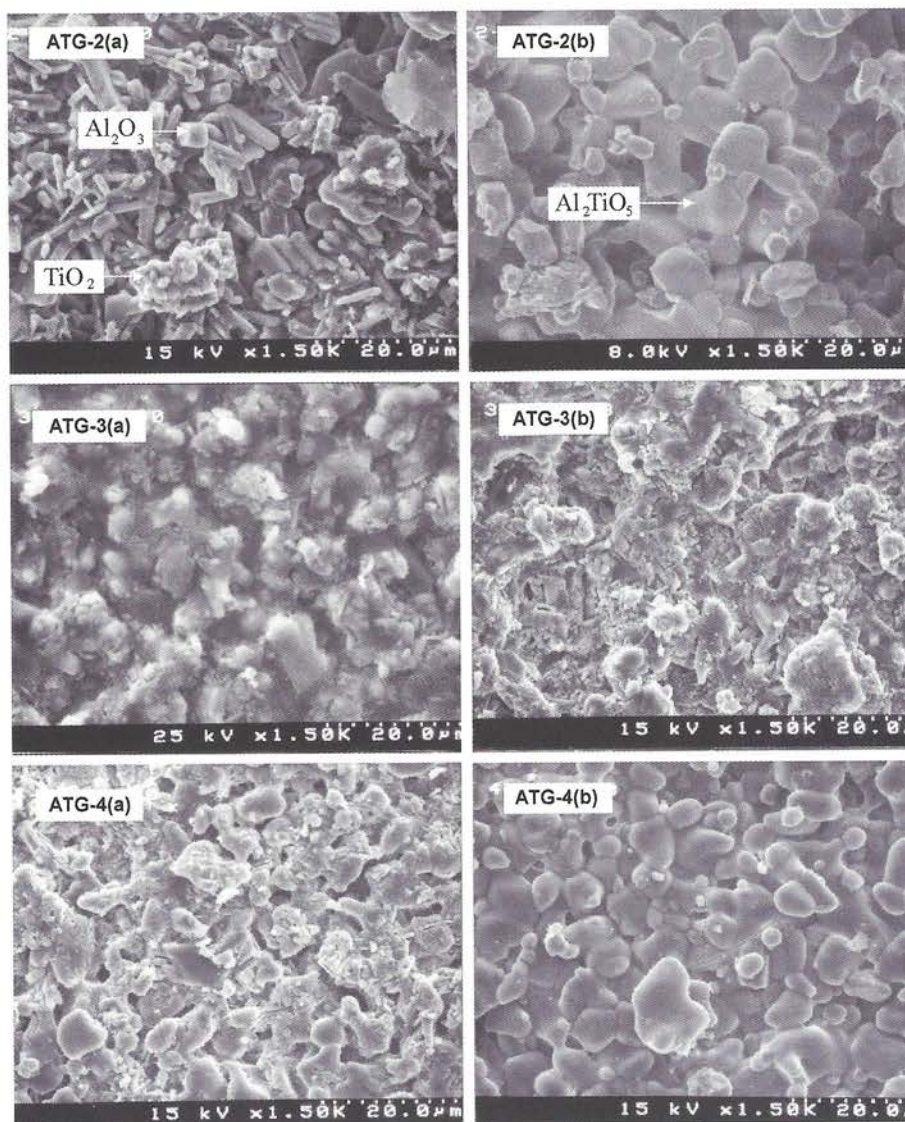


Fig. 2. Microstructure of sintered ATG2, 3 and 4 after decomposition test at 1100°C for 100 hrs (a) and cyclic thermal shock between 750-1400-750°C (b).

Table 3. Phase Composition of ATG Composites after Various Thermal Treatments<sup>12</sup>

Phase Composition	ATG-1 (unstabilized)	ATG-2 (unstabilized)	ATG-3 (fused stabilized)	ATG-4 (fused stabilized)
After Fusion Process	$\beta$ -AT	$\beta$ -AT	$\beta$ -AT	$\beta$ -AT $\alpha$ - $\text{Al}_2\text{O}_3$
Sintering at 1500°C/2 hrs	$\beta$ -AT	$\beta$ -AT	MA-Spinel m-ZrO <sub>2</sub> $\beta$ -AT $\alpha$ - $\text{Al}_2\text{O}_3$ Mullite m-ZrO <sub>2</sub>	MA-Spinel m-ZrO <sub>2</sub> $\beta$ -AT $\alpha$ - $\text{Al}_2\text{O}_3$ MA-Spinel m-ZrO <sub>2</sub>
Cyclic Thermal Shock Test (750-1400-750°C, 23 Cycles > 100 hrs)	$\beta$ -AT $\alpha$ - $\text{Al}_2\text{O}_3$ Rutile	$\beta$ -AT $\alpha$ - $\text{Al}_2\text{O}_3$ Rutile	$\beta$ -AT $\alpha$ - $\text{Al}_2\text{O}_3$ Mullite m-ZrO <sub>2</sub> $\beta$ -AT $\alpha$ - $\text{Al}_2\text{O}_3$ Rutile MA-Spinel Mullite m-ZrO <sub>2</sub>	$\beta$ -AT $\alpha$ - $\text{Al}_2\text{O}_3$ MA-Spinel m-ZrO <sub>2</sub> $\beta$ -AT $\alpha$ - $\text{Al}_2\text{O}_3$ Rutile MA-Spinel m-ZrO <sub>2</sub>
Decomposition Test [Annealing at 1100°C for 100 hrs.]	$\alpha$ - $\text{Al}_2\text{O}_3$ Rutile	$\alpha$ - $\text{Al}_2\text{O}_3$ Rutile	$\beta$ -AT $\alpha$ - $\text{Al}_2\text{O}_3$ Rutile MA-Spinel Mullite m-ZrO <sub>2</sub>	$\beta$ -AT $\alpha$ - $\text{Al}_2\text{O}_3$ Rutile MA-Spinel m-ZrO <sub>2</sub>

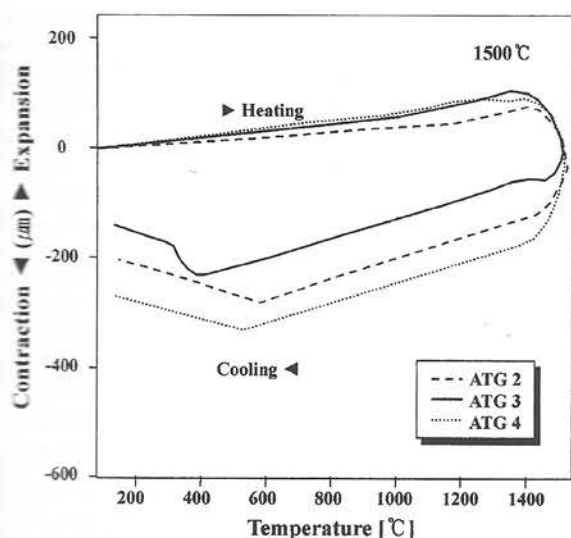


Fig. 3. Thermal expansion curves of sintered ATG2, 3 and 4 at 1500°C for 2 hrs.

cracks are closed, the steeper the thermal expansion curve. However, even at 1200°C the slope is far below the theoretical value, suggesting that a lot of fraction of the microcracks is still open.

The thermal expansion curves of ATG2, ATG3 and ATG4 demonstrated nearly the same hysteresis with internal rupture or microcracking created during cooling (Fig. 3). The microcracking existing in the material is responsible for the low mechanical strength on the one hand and on the other hand they give the material a kind of quasi-elasticity. The difference in the microcracking temperature, such as 587.6, 405.0 and 519.7 °C, for the specimens ATG2, ATG3 and ATG4 respectively, was caused by the difference in grain size of  $\beta$ - $\text{Al}_2\text{TiO}_5$  and additive content.

The thermal expansion of ATG materials after cyclic test in 23 cycles gives a slight smaller hysteresis area and higher thermal expansion in Fig. 4. It can be clearly indicated that the onset of decomposition of  $\text{Al}_2\text{TiO}_5$  into its component oxides (see Table 3) in Fig. 5 demonstrates another thermal expansion behavior of ATG materials after decomposition test at 1100°C for 100 hrs. This result can be also attributed to decomposition into  $\alpha$ - $\text{Al}_2\text{O}_3$  and  $\text{TiO}_2$  (rutile).

Table 4 shows the effect of sintering temperature on the densification, the thermal expansion behavior and the grain size of  $\text{Al}_2\text{TiO}_5$ . The coefficients of ATG3 were between  $0.83 \times 10^{-6}$  and  $4.71 \times 10^{-6}/\text{K}$  (RT-1500 °C) only, much smaller compared with the theoretical thermal expansion coefficient for dense  $\text{Al}_2\text{TiO}_5$  ceramics,  $9.7 \times 10^{-6}/\text{K}$ .

As shown in Fig. 6, the Young's modulus was measured as a function of quenching number by the resonance method. ATG3 having 7.90%  $\text{SiO}_2$  has relatively higher Young's modulus of 34 kN/mm<sup>2</sup> than the others. However, it shows sudden decrease of Young's modulus after one quenching cycle, but had

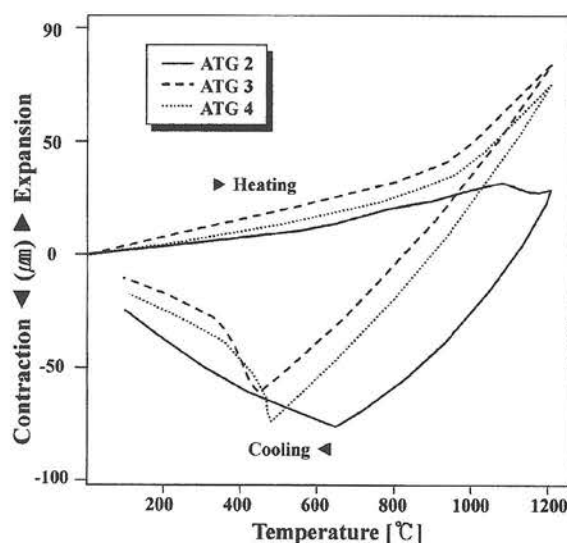


Fig. 4. Thermal expansion curves of ATG2, 3 and 4 after cyclic thermal shock test between 750-1400-750°C.

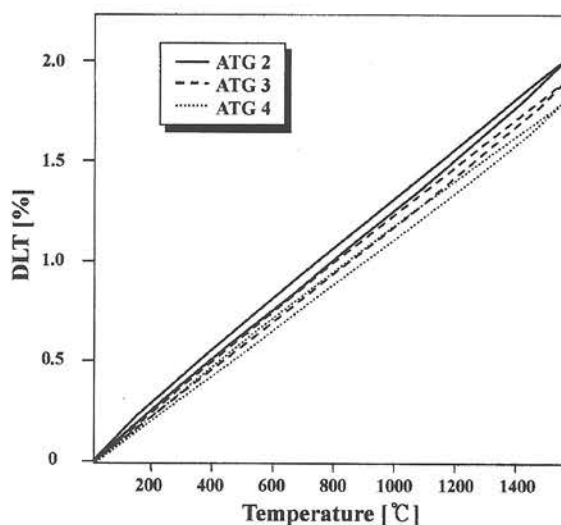


Fig. 5. Thermal expansion curves of ATG2, 3 and 4 after decomposition test at 1100°C for 100 hrs.

moderate thermal shock resistance. According to basic finding, higher microcrack densities and porosity of 4.7~6.8% in ATG materials also have positive effects on resistance to damage due to critical thermal shock. These can be attributed to grain boundary microcracks as a stress absorber [12].

Table 5 shows the effect of  $\text{MgO}$ ,  $\text{SiO}_2$  and  $\text{ZrO}_2$  contents on the Young's modulus, thermal expansion coefficient, flexural strength and the thermal-stress-resistance factor ( $R_1$ ,  $R_2$ ).  $\text{SiO}_2$  additions of 7.90 wt% did improve the strength of ATG3 to 50.0 MPa with a low thermal expansion coefficient of  $1.0 \times 10^{-6} \text{ K}^{-1}$ . This was attributed to the formation of a grain boundary liquid phase during sintering which aided densification and thus reduce microcracking, thereby increasing the strength. This result was presented with the higher calculated value of  $R_1$  (1029) and  $R_2$  (1544).

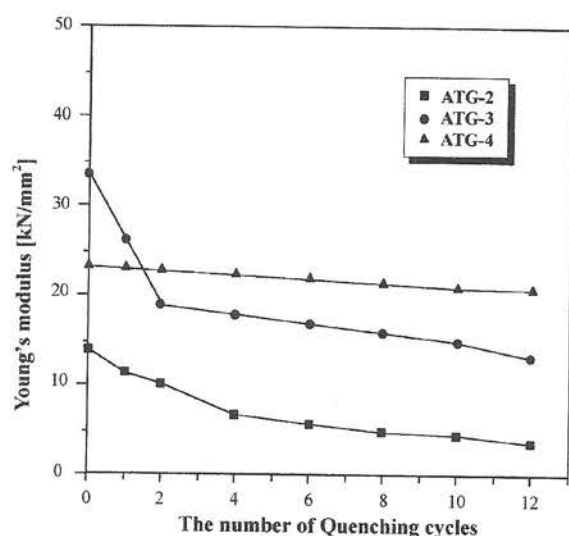


**Table 4.** The Densification, the Thermal Expansion Behavior and the Grain Size of ATG Ceramics, after Sintered Various Temperature

Materials	Sintering temperature (2 hrs)	Relative density (%)	Grain size ( $\mu\text{m}$ )	Maximum expansion (%)	Thermal expansion coefficient $\alpha_{25-1000^\circ\text{C}}$ ( $10^{-6} \text{ K}^{-1}$ )	Microcracking Temp. ( $^\circ\text{C}$ )
ATG2	1400 $^\circ\text{C}$	94.72	3~12 $\mu\text{m}$			0
	1450 $^\circ\text{C}$	94.80	3~15 $\mu\text{m}$	0.40	3.00	580.7
	1500 $^\circ\text{C}$	94.42	5~15 $\mu\text{m}$	0.40	2.45	587.6
	1550 $^\circ\text{C}$	93.78	5~17 $\mu\text{m}$	0.26	1.18	619.10
ATG3	1400 $^\circ\text{C}$	92.43	2~7 $\mu\text{m}$	0.80	4.71	0
	1450 $^\circ\text{C}$	95.30	2~7 $\mu\text{m}$	0.50	3.28	402.1
	1500 $^\circ\text{C}$	92.40	10 $\mu\text{m}$	0.50	2.35	405.0
	1550 $^\circ\text{C}$	92.86	10~20 $\mu\text{m}$	0.30	0.83	467.0
ATG4	1400 $^\circ\text{C}$	94.95	2~5 $\mu\text{m}$	0.51	4.02	480.8
	1450 $^\circ\text{C}$	95.10	2~5 $\mu\text{m}$	0.41	2.56	497.4
	1500 $^\circ\text{C}$	94.85	5~10 $\mu\text{m}$	0.41	2.79	519.7
	1550 $^\circ\text{C}$	92.10	10~15 $\mu\text{m}$	0.40	1.22	611.3

**Table 5.** Characteristics of Specimens of ATG Composites after heat Treatment at 1500 $^\circ\text{C}$  for 2 hrs

Materials	Flexural strength $\delta_{br}$ (N/mm $^2$ )	Young's modulus E (kN/mm $^2$ )	Thermal Expansion Coefficient 20-1000 $^\circ\text{C}$ ( $10^{-6}/\text{K}^{-1}$ )	R <sub>1</sub> (k)	R <sub>2</sub> (W/m)
ATG-2	25	14	5	833	1249
ATG-3	50	34	1.0	1029	1544
ATG-4	29	22.5	1.0	902	1353

**Fig. 6.** Young's modulus of ATG materials with thermal shock in the water quench.

This conclusion was reached from the low Young's modulus, low strength and low thermal expansion coefficient ( $1.0\sim 1.5 \times 10^{-6} \text{ K}^{-1}$ ) of ATG composites caused by presence of microfissures.

### Conclusions

The thermal instability of  $\text{Al}_2\text{TiO}_5$  ceramics was controlled by solid solution with  $\text{MgO}$ ,  $\text{SiO}_2$ , and  $\text{ZrO}_2$

through electrofusion in an arc furnace. The thermal expansion properties of  $\text{Al}_2\text{TiO}_5$  composites show the hysteresis due to the strong anisotropy of the crystal axes of these material. These phenomena are explained by the opening and closing of microcracks. The difference in microcracking temperatures, e.g. 587.6 (ATG2), 405.9 (ATG3) and 519.7 $^\circ\text{C}$  (ATG4) is caused by the difference in grain size and stabilizer type. The thermal shock behavior under cyclic conditions between 750-1400-750 $^\circ\text{C}$  shows no change in microstructure and phase assemblage for all three stabilized specimens. After the thermal loading test at 1100 $^\circ\text{C}$  for 100 hrs, ATG1 and ATG2 materials decomposes completely to its components corundum and rutile in both cases.

### References

1. X.G. Chen and S. Engler "Untersuchung des Kristallisationsblaus von berweredelten Aluminium Silizium Legierungen mit Hife der thermischen Anaylse", Giesserei, 77, 2, 49-54 (1990)
2. H. Nink, H. Keller, and A. Krauth, "Keramische Werkstoffe fuer das Giessen und schmelzen von Aluminium und Aluminiumlegierungen", Giesserei 64 (1977) 282-283.
3. F.C. Dimayuga "Veredelung von Aluminium-Silium-Legierungen mit Strontium, Natrium und Antimon" Giesserei-Praxis, 23/24 (1991) 309-397.
4. E. Gugel, "Keramische konstruktionswerkstoffe fuer den Motorenbau", Keram. Zeitschrift, 36, 9 (1984) 477-479.
5. W.D. Grunde, "Keramische Isolationsbauteile fuer Motoren", in: Keramische Hochleistungsbauteile fuer den Motoren

- und Triebwerksbau, VDI-Verlag, Duesseldorf, Zeitschrift fuer Werkstofftechnik, 26-35 (1985).
6. K. Uppenbrock, "Keramik in Motoren und Gasturbinen", Sprechsaal, 121. 2 (1988) 35-139.
7. Morosin and R.W. Lynch, "Structure studies on  $Al_2TiO_5$  at room temperature and at 600", Acta Cryst, B28 (1972) 1040.
8. E. Kato, K. Daimon, and I. Takahashi, "Decomposition kinetics of  $Al_2TiO_5$  in powdered state", J. Am. Ceram. Soc. 63 (1980) 355.
9. H.A.J. Thomas, and R. Sterens, "Aluminium titanate-A literature review, part I: microcracking phenomena" Br. Ceram. Trans. J. 88 (1989) 144.
10. D. Munz, and T. Fett, "Mechanisches Verhalten keramischer Werkstoffe, Werkstoff-Forschung und -technik", Herausgegeben von B. Iischer Band 8 Springer-Verlag, (1989).
11. I.J. Kim, "Anwendung des Sol-Gel-Verfahrens auf die Herstellung keramischer Werkstoffe aus Aluminiumtitanat-Mullit, Dissertation, Institut fuer Gesteins huttenkunde, Techn. University Aachen, Germany (1991).
12. W. Staudt, "Eigenschaften, Korrosionsverhalten und moegliche Anwendungen von geschmolzenem Aluminiumtitanat", Dissertation, RWTH Aachen (1988).